PROCEEDINGS of the
23rd International Congress on Acoustics
9 to 13 September 2019 in Aachen, Germany

Three-dimensional spatial active noise control based on kernel-induced sound field interpolation

Hayato ITO[(1)], Shoichi KOYAMA[(1),(2)], Natsuki UENO[(1)], Hiroshi SARUWATARI[(1)]

[(1)]The University of Tokyo, Graduate School of Information Science and Technology, Japan, hayato_ito@ipc.i.u-tokyo.ac.jp
[(2)]JST, PRESTO, Japan

Abstract

A method for feedback active noise control (ANC) over a three-dimensional (3D) spatial region is proposed. Conventional multipoint ANC does not guarantee to reduce the noise between multiple discrete control points. Several attempts have been made to reduce the noise over the continuous target region. Most methods for spatial ANC found their basis on the spherical/cylindrical harmonic expansion of the sound field. Therefore, they can be applied only for arrays of simple geometries such as sphere and cylinder. We propose a 3D spatial ANC method based on sound field interpolation, which can be applied to arbitrary array geometries. The mathematical principle of the proposed method is based on our recent studies on kernel ridge regression for sound field interpolation. The difference in the resulting algorithm from the general adaptive control appears only in the weighting matrix for error signals, which can be computed in advance only by using the relative positions of the microphones and the target region. Numerical simulation results indicated that a large regional noise reduction is achieved by the proposed method compared with conventional multipoint ANC.

Keywords: Active noise control, Sound field interpolation, Sound field control, Kernel method

1 INTRODUCTION

Active noise control (ANC), or active noise cancellation, aims to cancel incoming primary noise by using secondary actuators (loudspeakers) (1, 2). ANC has been mainly investigated for reducing the noise at predefined single or multiple control points using adaptive control techniques when the noise sources and secondary loudspeakers are placed apart from a target control region. Many practical ANC systems have also been developed based on these techniques (3, 4, 5, 6).

Multichannel ANC algorithms, where multiple secondary loudspeakers are used for controlling noise at multiple positions, have been developed both in time and frequency domains in the literature (7). The power of the error microphones placed at the control points is generally used as the cost function, and a type of least-mean-square (LMS) algorithms is typically applied for the adaptive control. Two types of adaptive control have been investigated: feedforward and feedback control (8). The feedforward ANC system is applicable to reduce nonstationary noise by using reference microphones. The feedback ANC is effective for periodic noise signals without using the reference microphones. The main drawback of the multichannel ANC is its limitation of the noise cancellation only on the multiple discrete positions; therefore, the region between the error microphones is not taken into consideration.

Sound field recording and reproduction have been investigated for reconstructing a spatial sound field both in the theoretical analysis (9, 10, 11, 12) and development of practical systems (13, 14). In recent years, these studies have led to researches on spatial ANC, which aims to cancel spatial noise in a continuous target region. Most methods of the spatial ANC is generally based on the spherical/circular harmonic expansions of the sound field inside the target region (15, 16, 17, 18); however, they can only be applied to simple array geometry such as sphere and cylinder.

We propose a method for three-dimensional (3D) spatial ANC using distributed microphones and loudspeakers, which is based on the interpolation using kernel ridge regression with the constraint that the function to be estimated satisfies the Helmholtz equation in the frequency domain (19, 20). We recently proposed a feedforward

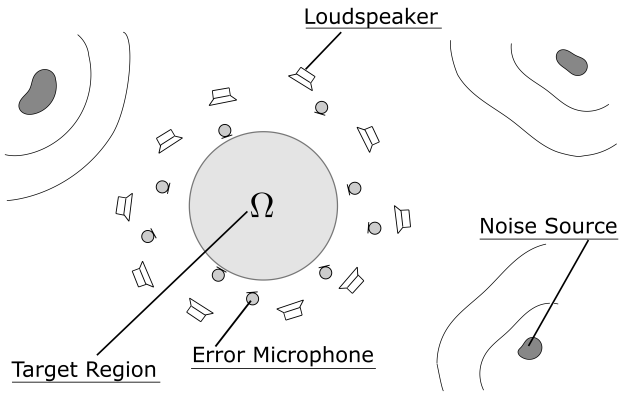

Figure 1. Arrangement of secondary loudspeakers and error microphones in feedback spatial ANC

spatial ANC in 2D on the basis of the kernel-induced sound field interpolation (21). In this paper, we formulate a feedback spatial ANC method, which aims to reduce periodic noise inside a 3D target region. The spatial noise reduction performance of the proposed method is evaluated by numerical simulations compared with the multipoint feedback control.

2 FEEDBACK ACTIVE NOISE CONTROL BASED ON NLMS ALGORITHM

We first revisit the multichannel feedback control based on the normalized LMS (NLMS) algorithm in the frequency domain. The objective is to reduce the spatial noise from primary noise sources inside a target region Ω by using multiple microphones and loudspeakers as shown in Fig. 1. L secondary loudspeakers and M error microphones are arranged around Ω, and the loudspeaker output is determined by an adaptive algorithm to cancel the primary noise field. The driving signals of the loudspeakers and the signals of the error microphones at the angular frequency ω are denoted as $\boldsymbol{d}(\omega) \in \mathbb{C}^L$ and $\boldsymbol{e}(\omega) \in \mathbb{C}^M$, respectively. We hereafter omit ω for notational simplicity. When the sound pressures of the primary noise field at the positions of the error microphones are denoted as $\boldsymbol{u}_\mathrm{p} \in \mathbb{C}^M$, the signals of the error microphones are represented as

$$\boldsymbol{e} = \boldsymbol{G}\boldsymbol{d} + \boldsymbol{u}_\mathrm{p}, \tag{1}$$

where $\boldsymbol{G} \in \mathbb{C}^{M\times L}$ is the transfer function matrix from the secondary loudspeakers to the error microphones. We assume that $\boldsymbol{G}$ is given by measurements in advance.

The multipoint pressure control (MPC) for the feedback ANC aims to minimize the square ℓ_2-norm of the error signals (7). Thus, the cost function of MPC $\mathscr{J}_\mathrm{MPC}$ is formulated as

$$\mathscr{J}_\mathrm{MPC} = \|\boldsymbol{e}\|_2^2 = \boldsymbol{e}^\mathsf{H}\boldsymbol{e}, \tag{2}$$

where the superscript $(\cdot)^\mathsf{H}$ denotes the conjugate transpose. In the complex LMS algorithm, the driving signals of the loudspeakers are adaptively determined by updating in the steepest-descent direction of $\mathscr{J}_\mathrm{MPC}$ at each step as

$$\begin{aligned}\boldsymbol{d}(n+1) &= \boldsymbol{d}(n) - \eta \frac{\partial}{\partial \boldsymbol{d}^*}\mathscr{J}_\mathrm{MPC} \\ &= \boldsymbol{d}(n) - \eta \boldsymbol{G}^\mathsf{H}\boldsymbol{e}(n)\end{aligned} \tag{3}$$

where the superscript $(\cdot)^*$ denotes the complex conjugate, n denotes the iteration index, and η is the step size parameter. The complex NLMS algorithm (22) is frequently used for faster convergence in which $\boldsymbol{d}$ is updated

as

$$\boldsymbol{d}(n+1) = \boldsymbol{d}(n) - \frac{\eta_0}{\|\boldsymbol{G}^{\mathsf{H}}\boldsymbol{G}\|_2 + \varepsilon}\boldsymbol{G}^{\mathsf{H}}\boldsymbol{e}(n), \tag{4}$$

where $\varepsilon > 0$ is the regularization parameter and $\eta_0 \in (0,2)$ is the normalized step size parameter.
We here introduce a weighting matrix to the cost function. The cost function $\mathscr{J}$ of the square ℓ_2-norm of $\boldsymbol{e}$ with the weighting matrix $\boldsymbol{A} \in \mathbb{C}^{M\times M}$, which is independent of $\boldsymbol{d}$, is represented as

$$\mathscr{J} = \boldsymbol{e}^{\mathsf{H}}\boldsymbol{A}\boldsymbol{e}. \tag{5}$$

The NLMS algorithm for $\mathscr{J}$ can be obtained in a similar manner to the case of $\mathscr{J}_{\mathrm{MPC}}$ as

$$\boldsymbol{d}(n+1) = \boldsymbol{d}(n) - \frac{\eta_0}{\|\boldsymbol{G}^{\mathsf{H}}\boldsymbol{A}\boldsymbol{G}\|_2 + \varepsilon}\boldsymbol{G}^{\mathsf{H}}\boldsymbol{A}\boldsymbol{e}(n). \tag{6}$$

Our proposed method, which is discussed in the next section, is based on the NLMS algorithm using the weighted-square-ℓ_2-norm. Note that the computational cost for the filter update in Eq. (6) is exactly the same as that in Eq. (4) by calculating $\boldsymbol{G}^{\mathsf{H}}\boldsymbol{A}$ and $\|\boldsymbol{G}^{\mathsf{H}}\boldsymbol{A}\boldsymbol{G}\|_2$ in advance. The specific $\boldsymbol{A}$ for 3D spatial ANC is given in the following section.

3 3D SPATIAL ANC BASED ON KERNEL-INDUCED SOUND FIELD INTERPOLATION

Our objective is to reduce the primary noise in the entire target region Ω. However, in the conventional MPC, the noise only at the positions of the error microphones is reduced, and the region between these microphones is not taken into consideration. We consider the regional noise power for the cost function as in our previously proposed method for feedforward control (21) as

$$\mathscr{L} = \int_{\Omega} |u_{\mathrm{e}}(\boldsymbol{r})|^2 \,\mathrm{d}\boldsymbol{r}, \tag{7}$$

where $u_{\mathrm{e}}(\boldsymbol{r})$ is the continuous pressure field at the position $\boldsymbol{r}$, which is the superposition of the primary noise field and the sound field synthesized by the secondary loudspeakers. Obviously, it is impractical to directly obtain $u_{\mathrm{e}}(\boldsymbol{r})$ by densely arranging the error microphones inside Ω. We apply the kernel interpolation technique for the sound field (19, 20) to estimate $u_{\mathrm{e}}(\boldsymbol{r})$ from the error signals $\boldsymbol{e}$.

3.1 Weighting matrix for 3D sound field interpolation

A method for estimating spherical harmonic coefficients at an arbitrary position from the pressure measurements of distributed microphones was proposed by Ueno *et al.* (20), which is based on the spherical harmonic analysis of infinite order of a sound field. This method can be regarded as the kernel ridge regression for sound field interpolation (19). We apply this method to estimate $u_{\mathrm{e}}(\boldsymbol{r})$ from $\boldsymbol{e}$. When Ω does not include any sources and the error microphones are omnidirectional, the estimate $\hat{u}_{\mathrm{e}}(\boldsymbol{r})$ can be obtained as

$$\hat{u}_{\mathrm{e}}(\boldsymbol{r}) = \left((\boldsymbol{K} + \lambda\boldsymbol{I})^{-1}\boldsymbol{e}\right)^{\mathsf{T}}\boldsymbol{\kappa}(\boldsymbol{r}), \tag{8}$$

where the superscript $(\cdot)^{\mathsf{T}}$ denotes the transpose, $\boldsymbol{I}$ is the identity matrix, λ is the regularization parameter. Here, $\boldsymbol{K}$ and $\boldsymbol{\kappa}$ for 3D sound field interpolation are defined as

$$\boldsymbol{K} = \begin{bmatrix} j_0(k\|\boldsymbol{r}_1 - \boldsymbol{r}_1\|) & \cdots & j_0(k\|\boldsymbol{r}_1 - \boldsymbol{r}_M\|) \\ \vdots & \ddots & \vdots \\ j_0(k\|\boldsymbol{r}_M - \boldsymbol{r}_1\|) & \cdots & j_0(k\|\boldsymbol{r}_M - \boldsymbol{r}_M\|) \end{bmatrix} \tag{9}$$

and

$$\boldsymbol{\kappa}(\boldsymbol{r}) = [j_0(k\|\boldsymbol{r}-\boldsymbol{r}_1\|), \cdots, j_0(k\|\boldsymbol{r}-\boldsymbol{r}_M\|)]^{\mathsf{T}}, \tag{10}$$

respectively, where $j_0(\cdot)$ is the zeroth-order spherical Bessel function of the first kind, $k = \omega/c$ is the wave number with the sound speed c, and $\boldsymbol{r}_m$ ($m \in \{1, \cdots, M\}$) is the position of the mth error microphone. Note that the interpolant is determined only by the relative positions of the error microphones without setting the expansion center and truncation order of the harmonic coefficients required in the general spherical-harmonic-expansion-based methods.

By substituting Eq. (8) into Eq. (7), the cost function $\mathscr{L}$ can be written as

$$\mathscr{L} = \int_{\Omega} |\hat{u}_{\mathrm{e}}(\boldsymbol{r})|^2 \mathrm{d}\boldsymbol{r} = \boldsymbol{e}^{\mathsf{H}} \boldsymbol{A} \boldsymbol{e}, \tag{11}$$

where

$$\boldsymbol{A} = \boldsymbol{P}^{\mathsf{H}} \left(\int_{\Omega} \boldsymbol{\kappa}^*(\boldsymbol{r}) \boldsymbol{\kappa}^{\mathsf{T}}(\boldsymbol{r}) \mathrm{d}\boldsymbol{r} \right) \boldsymbol{P} \tag{12}$$

and $P \equiv (\boldsymbol{K} + \lambda \boldsymbol{I})^{-1}$. Since $\mathscr{L}$ in Eq. (11) has the form of the weighted ℓ_2-norm of $\boldsymbol{e}$ as in Eq. (5), and $\boldsymbol{A}$ in Eq. (12) is independent of $\boldsymbol{d}$, the NLMS algorithm in Eq. (6) can be applied.

3.2 Efficient computation of weighting matrix for spherical target region

When the target region Ω is spherical, it is possible to avoid the computation of the numerical integration in $\boldsymbol{A}$. The radius of the spherical region Ω is denoted as R. First, in spherical coordinates $\boldsymbol{r} = (r, \theta, \phi)$, addition theorem for spherical Bessel function is expressed as (23)

$$\begin{aligned} j_0(k\|\boldsymbol{r}-\boldsymbol{r}_m\|) &= 4\pi \sum_{\nu=0}^{\infty} \sum_{\mu=-\nu}^{\nu} (-1)^{\nu} j_{\nu}(kr_m) Y_{\nu}^{\mu *}(-\hat{\boldsymbol{r}}_m) j_{\nu}(kr) Y_{\nu}^{\mu}(\hat{\boldsymbol{r}}) \\ &\equiv 4\pi \sum_{\nu=0}^{\infty} \xi_{\nu,m}(\boldsymbol{r}), \end{aligned} \tag{13}$$

where $\xi_{\nu,m}(\boldsymbol{r})$ is defined as

$$\xi_{\nu,m}(\boldsymbol{r}) = \underbrace{(-1)^{\nu} j_{\nu}(kr_m) \begin{pmatrix} Y_{\nu}^{-\nu}(-\hat{\boldsymbol{r}}_m) & Y_{\nu}^{-\nu+1}(-\hat{\boldsymbol{r}}_m) & \cdots & Y_{\nu}^{\nu}(-\hat{\boldsymbol{r}}_m) \end{pmatrix}^*}_{\boldsymbol{\alpha}_{\nu,m}} \underbrace{\begin{pmatrix} Y_{\nu}^{-\nu}(\hat{\boldsymbol{r}}) \\ \vdots \\ Y_{\nu}^{\nu}(\hat{\boldsymbol{r}}) \end{pmatrix} j_{\nu}(kr)}_{\boldsymbol{\beta}_{\nu}(\boldsymbol{r})} \equiv \boldsymbol{\alpha}_{\nu,m} \boldsymbol{\beta}_{\nu}(\boldsymbol{r}), \tag{14}$$

and $Y_{\nu}^{\mu}(\cdot)$ is the spherical harmonic function of νth order and μth degree. Here, $\hat{\boldsymbol{r}}$ represents the unit vector pointing to $\boldsymbol{r}$, i.e., $\hat{\boldsymbol{r}} = \boldsymbol{r}/\|\boldsymbol{r}\|_2$. Thus, $j_0(k\|\boldsymbol{r}-\boldsymbol{r}_m\|)$ can be written as

$$j_0(k\|\boldsymbol{r}-\boldsymbol{r}_m\|) = 4\pi \begin{pmatrix} \boldsymbol{\alpha}_{0,m} & \boldsymbol{\alpha}_{1,m} & \cdots \boldsymbol{\alpha}_{k,m} \cdots \end{pmatrix} \begin{pmatrix} \boldsymbol{\beta}_0(\boldsymbol{r}) \\ \boldsymbol{\beta}_1(\boldsymbol{r}) \\ \vdots \\ \boldsymbol{\beta}_k(\boldsymbol{r}) \\ \vdots \end{pmatrix}. \tag{15}$$

By substituting Eq. (15) into Eq. (10), $\boldsymbol{\kappa}(\boldsymbol{r})$ is represented as

$$\boldsymbol{\kappa}(\boldsymbol{r}) = 4\pi \underbrace{\begin{pmatrix} \boldsymbol{\alpha}_{0,1} & \boldsymbol{\alpha}_{1,1} & \cdots & \boldsymbol{\alpha}_{k,1} & \cdots \\ \boldsymbol{\alpha}_{0,2} & \boldsymbol{\alpha}_{1,2} & \cdots & \boldsymbol{\alpha}_{k,2} & \cdots \\ \vdots & \vdots & \cdots & \vdots & \cdots \\ \boldsymbol{\alpha}_{0,M} & \boldsymbol{\alpha}_{1,M} & \cdots & \boldsymbol{\alpha}_{k,M} & \cdots \end{pmatrix}}_{\boldsymbol{S}^{\mathsf{T}}} \underbrace{\begin{pmatrix} \boldsymbol{\beta}_0(\boldsymbol{r}) \\ \boldsymbol{\beta}_1(\boldsymbol{r}) \\ \vdots \\ \boldsymbol{\beta}_k(\boldsymbol{r}) \\ \vdots \end{pmatrix}}_{\boldsymbol{\phi}(\boldsymbol{r})} \equiv \boldsymbol{S}^{\mathsf{T}} \boldsymbol{\phi}(\boldsymbol{r}). \tag{16}$$

Therefore, the integral term in $\boldsymbol{A}$ becomes

$$\boldsymbol{A} = \boldsymbol{P}^{\mathsf{H}} \boldsymbol{S}^{\mathsf{H}} \left(\int_{\Omega} \boldsymbol{\phi}^*(\boldsymbol{r}) \boldsymbol{\phi}^{\mathsf{T}}(\boldsymbol{r}) \, \mathrm{d}\boldsymbol{r} \right) \boldsymbol{S}\boldsymbol{P}, \tag{17}$$

where

$$\begin{aligned} \boldsymbol{\phi}^*(\boldsymbol{r}) \boldsymbol{\phi}^{\mathsf{T}}(\boldsymbol{r}) &= \begin{pmatrix} \boldsymbol{\beta}_0(\boldsymbol{r}) \\ \boldsymbol{\beta}_1(\boldsymbol{r}) \\ \vdots \\ \boldsymbol{\beta}_k(\boldsymbol{r}) \\ \vdots \end{pmatrix}^* \begin{pmatrix} \boldsymbol{\beta}_0(\boldsymbol{r})^{\mathsf{T}} & \boldsymbol{\beta}_1(\boldsymbol{r})^{\mathsf{T}} & \cdots & \boldsymbol{\beta}_k(\boldsymbol{r})^{\mathsf{T}} & \cdots \end{pmatrix} \\ &= \begin{pmatrix} \boldsymbol{\beta}_0(\boldsymbol{r})^* \boldsymbol{\beta}_0(\boldsymbol{r})^{\mathsf{T}} & \boldsymbol{\beta}_0(\boldsymbol{r})^* \boldsymbol{\beta}_1(\boldsymbol{r})^{\mathsf{T}} & \cdots & \boldsymbol{\beta}_0(\boldsymbol{r})^* \boldsymbol{\beta}_j(\boldsymbol{r})^{\mathsf{T}} & \cdots \\ \boldsymbol{\beta}_1(\boldsymbol{r})^* \boldsymbol{\beta}_0(\boldsymbol{r})^{\mathsf{T}} & \boldsymbol{\beta}_1(\boldsymbol{r})^* \boldsymbol{\beta}_1(\boldsymbol{r})^{\mathsf{T}} & \cdots & \boldsymbol{\beta}_1(\boldsymbol{r})^* \boldsymbol{\beta}_j(\boldsymbol{r})^{\mathsf{T}} & \cdots \\ \vdots & \vdots & \ddots & \vdots & \cdots \\ \boldsymbol{\beta}_i(\boldsymbol{r})^* \boldsymbol{\beta}_0(\boldsymbol{r})^{\mathsf{T}} & \boldsymbol{\beta}_i(\boldsymbol{r})^* \boldsymbol{\beta}_1(\boldsymbol{r})^{\mathsf{T}} & \cdots & \boldsymbol{\beta}_i(\boldsymbol{r})^* \boldsymbol{\beta}_j(\boldsymbol{r})^{\mathsf{T}} & \cdots \\ \vdots & \vdots & \vdots & \vdots & \ddots \end{pmatrix} \end{aligned} \tag{18}$$

and

$$\boldsymbol{\beta}_i(\boldsymbol{r})^* \boldsymbol{\beta}_j(\boldsymbol{r})^{\mathsf{T}} = \begin{pmatrix} Y_i^{-i}(\hat{\boldsymbol{r}}) \\ \vdots \\ Y_i^{i}(\hat{\boldsymbol{r}}) \end{pmatrix}^* j_i^*(kr) j_j(kr) \begin{pmatrix} Y_j^{-j}(\hat{\boldsymbol{r}}) & \cdots & Y_j^{j}(\hat{\boldsymbol{r}}) \end{pmatrix}. \tag{19}$$

Owing to the orthogonality of the spherical Bessel functions, the integral term of this equation is derived as

$$\int_{\Omega} \boldsymbol{\phi}^*(\boldsymbol{r}) \boldsymbol{\phi}^{\mathsf{T}}(\boldsymbol{r}) \, \mathrm{d}\boldsymbol{r} = \mathrm{diag}(\gamma_0, \gamma_1, \gamma_1, \gamma_1, \gamma_2, \cdots) \equiv \boldsymbol{\Gamma}, \tag{20}$$

where

$$\gamma_\nu = \frac{R^3}{2} \left(j_\nu(kR)^2 - j_{\nu-1}(kR) j_{\nu+1}(kR) \right). \tag{21}$$

Here, a mathematical formula in Ref. (24) is used to derive Eq. (21). $2\nu+1$ elements of γ_ν is arranged for each ν as the diagonal components of $\boldsymbol{\Gamma}$. Finally, the weighting matrix $\boldsymbol{A}$ for the spherical target region Ω is derived as

$$\boldsymbol{A} = \boldsymbol{P}^{\mathsf{H}} \boldsymbol{S}^{\mathsf{H}} \boldsymbol{\Gamma} \boldsymbol{S} \boldsymbol{P}. \tag{22}$$

In practice, it is necessary to approximate the infinite matrices $\boldsymbol{S}$ and $\boldsymbol{\Gamma}$ as finite matrices of a sufficiently large size. Larger sizes of $\boldsymbol{S}$ and $\boldsymbol{\Gamma}$ are better for accurate numerical computation of the integration (25). Note that $\boldsymbol{A}$ can be calculated in advance only from the relative positions of the error microphones and the target region.

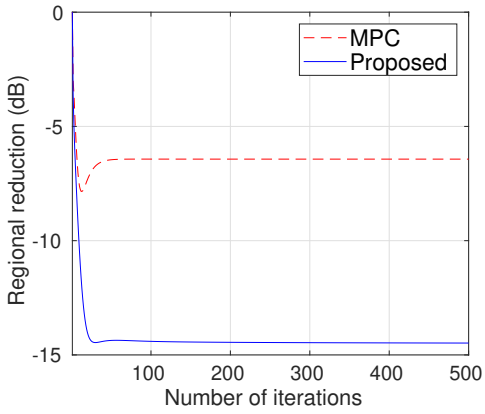

Figure 2. Regional noise power reduction inside Ω at 250 Hz with respect to number of iterations.

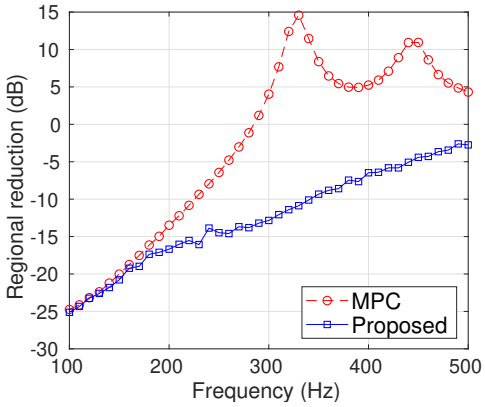

Figure 3. Regional noise power reduction inside Ω with respect to frequency.

4 NUMERICAL SIMULATIONS

Numerical simulations were conducted in a 3D sound field to compare the proposed method (**Proposed**) and multipoint pressure control (**MPC**). The target region Ω was set to be spherical with a radius of 0.5 m, and the coordinate origin was set at its center. $M = 60$ omnidirectional microphones were used as the error microphones. The secondary loudspeakers were assumed to be point sources and their number was $L = 30$. The error microphones were placed on three dual rings set on the surface of Ω. The intervals of the dual rings were 0.01 m. The three rings were set at $z = -0.3$, 0.0, and 0.3 m, respectively. On each ring, 10 error microphones were equiangularly placed. The secondary loudspeakers were placed on three rings set on the spherical surface of the radius 1.0 m. The three rings were at $z = -0.7$, 0.0, and 0.7 m, respectively. 10 secondary loudspeakers were equiangularly placed on each ring. The speed of sound was set as $c = 340$ m/s.

Six point sources were placed as the primary noise sources at $(-10.0, 0.0, 0.0)$, $(10.0, 0.0, 0.0)$, $(0.0, -10.0, 0.0)$, $(0.0, 10.0, 0.0)$, $(0.0, 0.0, -10.0)$ and $(0.0, 0.0, 10.0)$ m in Cartesian coordinates. The source signals were single-frequency complex sine waves. Observation noise was also added to the error microphones so that the signal-to-noise ratio (SNR) was 40 dB. For evaluation, the performance measure with regard to the regional noise power reduction inside Ω is defined as

$$P_{\mathrm{red}} = 10 \log_{10} \frac{\sum_i |u_{\mathrm{e}}^{(n)}(\boldsymbol{r}_i)|^2}{\sum_i |u_{\mathrm{e}}^{(0)}(\boldsymbol{r}_i)|^2}, \tag{23}$$

where $u_{\mathrm{e}}^{(n)}(\boldsymbol{r}_i)$ is the total pressure field at the ith evaluation position $\boldsymbol{r}_i$ for the nth iteration. The evaluation positions were obtained by discretizing Ω with intervals of 0.025 m. The pressure field at the zeroth iteration $u_{\mathrm{e}}^{(0)}(\boldsymbol{r}_i)$ was the original pressure field generated by the primary noise sources.

We first show the results when the frequency was set at 250 Hz and the amplitude of six noise sources was 10, 20, 30, 40, 50, and 60, respectively. The parameter ε was set as 10^{-2}. The maximum order ν used for constructing the matrices $\boldsymbol{S}$ and $\boldsymbol{\Gamma}$ was 40. The regularization parameter λ was set as 10^{-4}. The performance measure P_{red} is plotted with respect to the number of iterations for the two methods in Fig. 2. **Proposed** achieved larger noise power reduction than **MPC**.

Figure 3 shows P_{red} with respect to the frequency after 500 iterations. **Proposed** and **MPC** achieved similar noise reduction when the frequency was below 200 Hz. Above 200 Hz, **Proposed** outperformed **MPC**.

5 CONCLUSIONS

We proposed a feedback spatial ANC method using distributed secondary loudspeakers and error microphones, which is based on the kernel ridge regression of a 3D sound field with the constraint that the function to be estimated satisfies the Helmholtz equation. The cost of the 3D regional error power is defined, and the kernel-induced sound field interpolation is applied to calculate it. The resulting algorithm includes a weighting matrix for the error signals obtained in advance by using the relative positions of the microphones and the target region. Numerical simulation results indicated that the proposed method outperforms the conventional multipoint control in regional noise reduction.

ACKNOWLEDGEMENTS

This work was supported by JST PRESTO Grant Number JPMJPR18J4, and SECOM Science and Technology Foundation.

REFERENCES

[1] Nelson, P. A.; Elliott, S. J. Active control of sound, Academic Press, London, 1st edition, 1992.

[2] Fuller, C. R.; Elliott, S. J.; Nelson, P. A. Active Control of Vibration, Academic, San Diego, CA, USA, 1st edition, 1996.

[3] Kuo, S. M.; Mitra, S.; Gan, W.-S. Active noise control system for headphone applications, IEEE Trans. Control Syst. Technol., Vol. 14 (2), 2006, pp. 331–335.

[4] Kottayi, S.; Althomali, R.; Thasleema, T. M.; Narayanan, N. K. Active noise control for creating a quiet zone around mobile phone, Proceedings of Int. Conf. Comm., Signal Process. (ICCSP), Melmaruvathur, Apr. 2016, pp. 73–77.

[5] Sano H.; Inoue, T.; Takahashi, A.; Terai, K.; Nakamura, Y. Active control system for low-frequency road noise combined with an audio system, IEEE Trans. Speech Audio Process., Vol. 9 (7), 2001, pp. 755–763.

[6] Diaz, J.; Egaña, J. M.; Viñolas, J. A local active noise control system based on a virtual-microphone technique for railway sleeping vehicle applications, Mech. Syst. Signal Process., Vol. 20, (8), 2006, pp. 2259–2276.

[7] Elliot, S. J.; Stothers, I. M.; Nelson, P. A. A multiple error LMS algorithm and its application to the active control of sound and vibration, IEEE Trans. Acoust., Speech, Signal Process., Vol. 35 (10), 1987, pp. 1423–1434.

[8] Kuo S. M.; Morgan, D. R. Active noise control: A tutorial review, Proc. IEEE, Vol. 87 (6), 1999, pp. 943–973.

[9] Poletti, M. A. Three-dimensional surround sound systems based on spherical harmonics, J. Audio Eng. Soc., Vol. 53 (11), 2005, pp. 1004–1025.

[10] Ahrens J.; Spors, S. An analytical approach to sound field reproduction using circular and spherical loudspeaker distributions, Acta Acustica United with Acustica, Vol. 94, 2008, pp. 988–999.

[11] Koyama, S.; Furuya, K.; Hiwasaki, Y.; Haneda, Y. Analytical approach to wave field reconstruction filtering in spatio-temporal frequency domain, IEEE Trans. Audio, Speech, Lang. Process., Vol. 21 (4), 2013, pp. 685–696.

[12] Koyama, S.; Furuya, K.; Hiwasaki, Y.; Haneda, Y.; Suzuki, Y. Wave field reconstruction filtering in cylindrical harmonic domain for with-height recording and reproduction, IEEE/ACM Trans. Audio, Speech, Lang. Process., Vol. 22 (10), 2014, pp. 1546–1557.

[13] Brix, S.; Sporer, T.; Plogsties, J. Carrouso - an European approach to 3D-audio, Proceedings of 110th Conv. AES, Amsterdam, May 2001.

[14] Koyama, S.; Furuya, K.; Uematsu, H.; Hiwasaki, Y.; Haneda, Y. Real-time sound field transmission system by using wave field reconstruction filter and its evaluation, IEICE Transactions on Fundamentals of Electronics, Communications and Computer Sciences, Vol. E97-A (9), 2014, pp. 1840–1848.

[15] Spors, S.; Buchner, H. An approach to massive multichannel broadband feedforward active noise control using wave-domain adaptive filtering, Proceedings of IEEE Int. Workshop Appl. Signal Process. Audio Acoust. (WASPAA), New Paltz, Oct. 2007, pp. 171–174.

[16] Spors S.; Buchner, H.; Efficient massive multichannel active noise control using wave-domain adaptive filtering, Proceedings of Int. Symp. Commun. Control Signal Process. (ISCCSP), Malta, Mar. 2008, pp. 1480–1485.

[17] Zhang, J.; Zhang, W.; Abhayapala, T. D. Noise cancellation over spatial regions using adaptive wave domain processing, Proceedings of IEEE Int. Workshop Appl. Signal Process. Audio Acoust. (WASPAA), New Paltz, Oct. 2015.

[18] Zhang, J.; Abhayapala, T. D.; Zhang, W.; Samarasinghe, N.; Jiang, S. Active noise control over space: A wave domain approach, IEEE/ACM Trans. Audio, Speech, Lang. Process., Vol. 26 (4), 2018, pp. 774–786.

[19] Ueno, N.; Koyama, S.; Saruwatari, H. Kernel ridge regression with constraint of helmholtz equation for sound field interpolation, Proceedings of "IWAENC 2018; International Workshop on Acoustic Signal Enhancement", Tokyo, Sept. 2018.

[20] Ueno, N.; Koyama, S.; Saruwatari, H. Sound field recording using distributed microphones based on harmonic analysis of infinite order, IEEE Signal Process. Lett., Vol. 25 (1), 2018, pp. 135–139.

[21] Ito, H.; Koyama, S.; Ueno, N.; Saruwatari, H. feedforward spatial active noise control based on kernel interpolation of sound field, Proceedings of IEEE Int. Conf. Acoust., Speech, Signal Process. (ICASSP), Brighton, May 2019 (to appear).

[22] Slock, D. T. M. On the convergence behaviour of the LMS and the normalized LMS algorithms, IEEE Trans. Signal Process., Vol. 41 (9), 1993, pp. 2811–2825.

[23] Martin, P. A. Multiple Scattering: Interaction of Time-Harmonic Waves with N Obstacles, Cambridge University Press, New York, 1st edition, 2006.

[24] Anderson, C. A.; Teal, P. D.; Poletti, M. A. Spatial correlation of radial Gaussian and uniform spherical volume near-field source distributions, IEEE/ACM Trans. Audio, Speech, Lang. Process., Vol. 24 (1), 2016, pp. 143–150.

[25] Ueno, N.; Koyama, S.; Saruwatari, H. Listening-area-informed sound field reproduction based on circular harmonic expansion, Proceedings of IEEE Int. Conf. Acoust., Speech, Signal Process. (ICASSP), New Orleans, Mar. 2017, pp. 111–115.